Journal of Power Sources 196 (2011) 3129–3133

Contents lists available at ScienceDirect

Journal of Power Sources

journal homepage: www.elsevier.com/locate/jpowsour

Short communication

Fabrication and characterization of $Sm_{0.2}Ce_{0.8}O_{2-\delta}$–$Sm_{0.5}Sr_{0.5}CoO_{3-\delta}$ composite cathode for anode supported solid oxide fuel cell

Jen-Chen Chang, Maw-Chwain Lee*, Rung-Je Yang, Yang-Chuang Chang, Tai-Nan Lin, Chun-Hsiu Wang, Wei-Xin Kao, Lin-Song Lee

Chemical Engineering Division, Institute of Nuclear Energy Research, No. 1000, Wunhua Rd., Jiaan Village, Longtan Township, Taoyuan County 32546, Taiwan, ROC

ARTICLE INFO

Article history:
Received 27 October 2010
Received in revised form
14 December 2010
Accepted 14 December 2010
Available online 21 December 2010

Keywords:
Solid oxide fuel cell
Strontium-doped samarium cobaltate
AC-impedance

ABSTRACT

The $Sm_{0.5}Sr_{0.5}CoO_{3-\delta}$ (SSC) with perovskite structure is synthesized by the glycine nitrate process (GNP). The phase evolution of SSC powder with different calcination temperatures is investigated by X-ray diffraction and thermogravimetric analyses. The XRD results show that the single perovskite phase of the SSC is completely formed above 1100 °C. The anode-supported single cell is constructed with a porous Ni–yttria-stabilized zirconia (YSZ) anode substrate, an airtight YSZ electrolyte, a $Sm_{0.2}Ce_{0.8}O_{2-\delta}$ (SDC) barrier layer, and a screen-printed SSC–SDC composite cathode. The SEM results show that the dense YSZ electrolyte layer exhibits the good interfacial contact with both the Ni–YSZ and the SDC barrier layer. The porous SSC–SDC cathode shows an excellent adhesion with the SDC barrier layer. For the performance test, the maximum power densities are 464, 351 and 243 mW cm^{-2} at 800, 750 and 700 °C, respectively. According to the results of the electrochemical impedance spectroscopy (EIS), the charge-transfer resistances of the electrodes are 0.49 and 1.24 Ω cm^2, and the non charge-transfer resistances are 0.48 and 0.51 Ω cm^2 at 800 and 700 °C, respectively. The cathode material of SSC is compatible with the YSZ electrolyte via a delicate scheme employed in the fabrication process of unit cell.

1. Introduction

Solid oxide fuel cell (SOFC) has been considered as a highly efficient and environmentally friendly power generation device. The SOFC is composed of three components: a porous anode, an electrolyte with high densification, and a porous cathode. The materials used for the conventional SOFC are mainly focused on the yttria stabilized zirconia (YSZ) electrolyte, Ni/YSZ cermet as the anode and strontium doped lanthanum manganate (LSM) as the cathode. The YSZ-based SOFC requires operation at higher temperature (~1000 °C) and this leads to some problems, such as high temperature seal and the inter-diffusion between cell components. On the other hand, the SOFC with lower operation temperature (below 800 °C) will extend the range of materials and have the better reliability. The reduction of operating temperature can be achieved by either thinning the electrolyte layer or using the higher conductive electrolytes for oxygen ion, such as doped ceria oxides.

However, in an anode-supported SOFC, the cathode polarization resistance is the main contributor to overall cell resistance. When the operation temperature is decreased, the cathode becomes critical for the fuel cell performance since the activation energy of the cathodic reaction is large [1,2]. Hence, to develop a high performance cathode is important for the intermediate-temperature SOFC (IT-SOFC).

Strontium doped lanthanum manganate is commonly used as cathode material. It has a good thermal and chemical compatibility with YSZ electrolyte [3], but its performance rapidly decreases as the operating temperature is decreased. Recently, cobalt-containing oxides with perovskite-type structure have been used as IT-SOFC cathode material due to the higher ionic conductivity and catalytic activity, such as $La_{0.5}Sr_{0.5}CoO_{3-\delta}$ (LSC), $Sm_{0.5}Sr_{0.5}CoO_{3-\delta}$ (SSC), $La_{0.5}Sr_{0.5}Co_{0.2}Fe_{0.8}O_{3-\delta}$ (LSCF), and $Ba_{0.5}Sr_{0.5}Co_{0.8}Fe_{0.2}O_{3-\delta}$ (BSCF) [4–7].

BSCF cathode exhibits very low polarization resistance due to its high oxygen diffusion coefficient and yields maximum power density at low temperature [8]. However, its large thermal expansion coefficient and low electrical conductivity may mismatch with electrolyte and limit the cell performance [9]. LSC possesses high electronic conductivity and high oxygen ion conductivity over a wide temperature range [10]. However, it also has the large thermal expansion coefficient problem. Although its thermal expansion coefficient can be reduced by doping Co-site with Fe^{3+} (LSCF), but the Fe^{3+} doping will also decrease the ionic conductivity of LSC [11].

Among the materials, the SSC is regarded as one of the most promising cathode materials because it shows a higher ionic conductivity than that of LSM, exhibits extraordinary electronic conductivity than that of pure BSCF [12], reveals a good catalysis for oxygen reduction [13], and is particularly compatible with the

* Corresponding author. Tel.: +886 3 4711400x5930; fax: +886 3 4711411.
E-mail address: mclee@iner.gov.tw (M.-C. Lee).

0378-7753/$ – see front matter © 2010 Elsevier B.V. All rights reserved.
doi:10.1016/j.jpowsour.2010.12.036

electrolytes of GDC and LSGM [5,14]. Ishihara et al. [14] and Fukunaga et al. [15] also reported that the overpotential of dense SSC film is lower than that of the dense LSC film under the same condition and the oxygen adsorption–desorption rate of SSC is one order magnitude higher than that of LSC. The disadvantages of the SSC are its large thermal expansion coefficient and the high reactivity with YSZ electrolyte above 900 °C [16]. However, the large thermal expansion coefficient of SSC can be reduced by adding ceria to SSC, which also increase triple phase boundary and improve the electrical properties of SSC cathode [17]. The interfacial reaction of YSZ and SSC can be avoided by coating $Sm_{0.2}Ce_{0.8}O_{1.9}$ (SDC) barrier onto YSZ electrolyte as a functional layer to prevent the formation of an interfacial-insulating layer in this regard.

Nowadays, we have successfully fabricated the airtight electrolyte with thin film of YSZ onto anode supported SOFC via spin coating process [18–19]. In order to further enhance the electrochemical performance, the improvement of cathode electrode is one of the most concerning investigations. Hence, in this study, the SSC–SDC composite cathode layer is applied as the cathode electrode. The characterizations of the cell are conducted by the performance test and the analysis of the electrochemical impedance spectroscopy (EIS).

2. Experimental

2.1. Synthesis of powders

$Sm_{0.5}Sr_{0.5}CoO_{3-\delta}$ (SSC) powder was synthesized by the glycine nitrate combustion process. Stoichiometric amounts of $Sm(NO_3)_3{\cdot}6H_2O$ (99.9%), $Sr(NO_3)_2$(99.0%), and $Co(NO_3)_2{\cdot}6H_2O$ (98.5%) were dissolved in the distilled water to form an aqueous solution. The glycine solution was added into the solution to maintain a mole ratio of 1: 2 for the total metal ions to glycine. The solution was heated until a red viscous gel was formed. Then, the gel swelled and was subjected to the self-sustaining combustion. The resultant product was calcined at 1000 °C for 2 h to remove the residual carbon components and to form a crystalline structure.

$Sm_{0.2}Ce_{0.8}O_{1.9}$ (SDC) powder was prepared using sol–gel process. Stoichiometric amounts of $Ce(NO_3)_3{\cdot}6H_2O$ and $Sm(NO_3)_3{\cdot}6H_2O$ were dissolved in the D.I. water, and the citric acid was added into the mixed nitrate solution. The mole ratio of citric acid to total metal ions was set at 2:1. The mixture was heated and stirred at 90 °C to form a transparent gel, and then was subjected to calcination at different temperatures.

2.2. Fabrication of MEA

The detail fabricating procedures of the membrane electrode assembly (MEA) were described in our previous studies [18–19]. Anode green tapes were cut and assembled with an area of 50 mm × 50 mm and the thickness of 1000 μm. The anode green substrate was subjected to a hot-press process via a laminator for several times and further calcined at 1400 °C for 4 h. The thin YSZ electrolyte and SDC barrier were both fabricated by spin coating process. At first, the YSZ electrolyte was coated onto anode substrate and calcined at 1400 °C for 6 h. And then the SDC barrier was subsequently coated onto YSZ electrolyte and calcined with the same sintering profile of YSZ electrolyte. The composite cathode of 70 wt.% SSC and 30 wt.% SDC was printed onto the SDC barrier by a screen printer, and then calcined at 1000 °C for 2 h in air. Finally, the unit cell of NiO–YSZ/YSZ/SDC/SSC–SDC was obtained.

2.3. Characterizations and performance test of SOFC-MEA

Thermal gravimetric analysis (TGA) of the powder was carried out using an instrument (TGA/DTA, Linseis, L81/1750) with simultaneous differential thermal and thermo-gravimetry analyses in air. The phase identification of SSC powders was performed by X-ray diffraction (XRD, Bruker, D8 advance) using CuK radiation. The precursor powders were heated at a heating rate of 10 °C min^{-1} from 35 to 1200 °C. Microstructure of the single cell with YSZ film was examined by a field emission scanning electron microscopy (FE-SEM, Hitachi S-4800). The single cell of SOFC was tested in a cell housing consisting of alumina base with alumina flanges for gas distribution, and platinum and nickel meshes for cathode and anode current collections, respectively. Platinum wires were used as the current leads for cell voltage measurement. Air as an oxidant was available by the air supplier. Hydrogen humidified by a water bubbler was used as a fuel. The flow rates of fuel and oxidant were 335 and 670 ml min^{-1}, respectively. The electrochemical performance was measured at 700–800 °C. The measurements of electrochemical impedance spectroscopy (EIS) were carried out under open circuit operation using a frequency analyzer (Solarton 1260) at the frequency range of 10 mHz to 0.1 MHz.

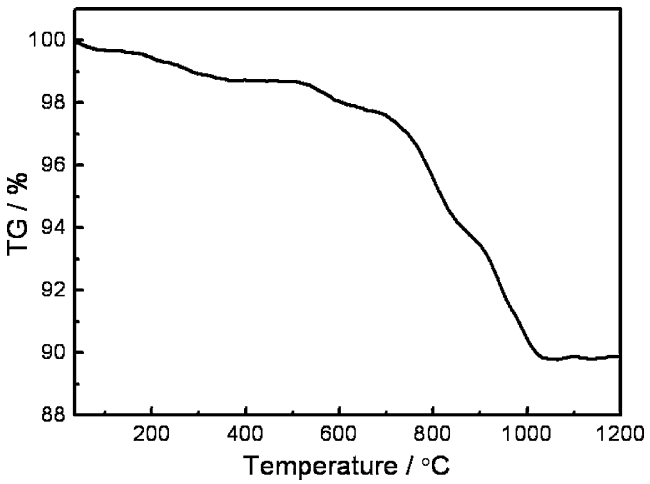

Fig. 1. TGA curve of the SSC powder measured at a heating rate of 10 °C min^{-1} in air.

3. Results and discussion

Fig. 1 shows the TGA curve of the SSC powder measured at a heating rate of 10 °C min^{-1} in air from 35 to 1200 °C. The TGA analysis shows that about 2% weight loss is observed at the temperature below 600 °C. This may be ascribed to the burning of the residue of organic materials in as-synthesized powder. With increase of the temperature, about 8% weight loss is observed from 600 to 1000 °C and that may attribute to the decomposition of carbonate and further crystallization of the perovskite phase. This result is in coincidence with that of our XRD analysis described later.

The XRD patterns of the SSC powders are shown in Fig. 2. The as-synthesized SSC powders were calcined in air for 2 h at various temperatures between 600 and 1200 °C to investigate the evolution of the crystalline phases. These diffraction peaks have been identified by the early studies [20–21]. The as-prepared powder and the powder calcined at 600 °C contain the corresponding oxides such as Sm_2O_3, Co_3O_4, and $SrCO_3$. These oxides subsequently react to form the SSC crystalline phase as the calcination temperature is increased. The main perovskite phase is observed from the powder calcined at 800 °C, but a minor amount of the $SrCO_3$ is still existed for the powder calcined at 800 and 900 °C. The completely single perovskite phase has been formed for the samples calcined over 1100 °C for 2 h. These results are in coincidence with the report by Bansal and Zhong [21].

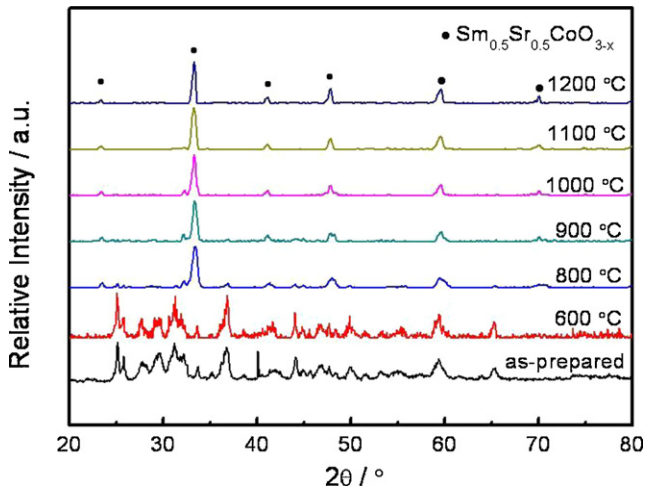

Fig. 2. XRD patterns of the SSC powders with various calcination temperatures.

In this work, the single cell consists of ~33 μm SSC–SDC cathode, ~5.8 μm SDC barrier, ~4.8 μm YSZ electrolyte and ~750 μm Ni–YSZ anode. The microstructures of the cross-section of the Ni–YSZ/YSZ/SDC/SSC–SDC cell are shown in Fig. 3. The YSZ electrolyte layer is dense and no crack or delamination is observed. It exhibits the good interfacial contact with both the Ni–YSZ and the SDC barrier. The porous SSC–SDC cathode shows an excellent adhesion with the SDC barrier due to the addition of SDC which can diminish the problem of the thermal expansion mismatch. The SDC barrier on the YSZ electrolyte is clearly visible and also has porous structure. However, according to Martínez-Amesti's report, the diffusion of $(SDC)_x(YSZ)_{1-x}$ phase was formed when SDC/YSZ powder mixture was sintered over 1100 °C in air [22]. For our case, an interface of reaction between YSZ and SDC can be discovered by the EDS technique. The result of EDS can clearly show that the ceria diffused into YSZ layer when the double electrolyte layers (SDC/YSZ) were sintered at 1400 °C for 6 h. The thickness of reaction layer was evaluated to be about 1.35 μm.

Fig. 4(a) shows the whole process of the cell performance test with time of over 200 h. Fig. 4(b) shows the I–*V* and *I*–*P* characteristics of the single cell. The open circuit voltages (OCVs) are 1.08, 1.10 and 1.11 V, and the maximum power densities are 464, 351 and 243 mW cm^{-2} at 800, 750 and 700 °C, respectively. The open circuit voltages are close to the theoretical value, which indicates that the thin film of YSZ deposited onto the porous Ni–YSZ anode is dense enough to prevent gas leakage through the electrolyte. In addition, the performance of the single cell is increased with the increase of the operation temperature. It indicates that the electrolyte resistance and the interfacial polarization are decreased with the increase of the operation temperature due to the diminution of oxygen conduction resistance and the increase of the catalytic activity.

AC impedance spectra of the cell at different temperatures are plotted in Fig. 5(a). The equivalent circuit and fitting results using the Zview program are given in Fig. 5(b) and summarized in Table 1. The cell impedance spectra consist of two clearly separated arcs in the frequency domain which indicates that molecular oxidation–reduction are controlled by at least two electrode processes. In the equivalent circuit, R_0 corresponds to the total ohmic resistance including the electrolyte, electrodes and connection wires; L is the inductance, which is attributed to the Pt current–voltage probes or the high-frequency phase shift of the electrochemical equipment. The resistance R_1 is the charge-transfer resistance, which is attributed to interfacial resistance between electrodes and electrolyte. The R_2 is the non charge-transfer process contributed by oxygen surface exchange, catalytic chemical reactions, solid-state diffusion, and gas-phase diffusion inside and outside the electrode [23]. The CPE_1 and CEP_2 are constant phase elements. From Table 1, it can be seen that both the R_0 and the R_1 increase with the decrease of the operating temperature, and the variation of the R_2 is much smaller than that of the R_0 and R_1.It indicates that both the interfacial resistance and total

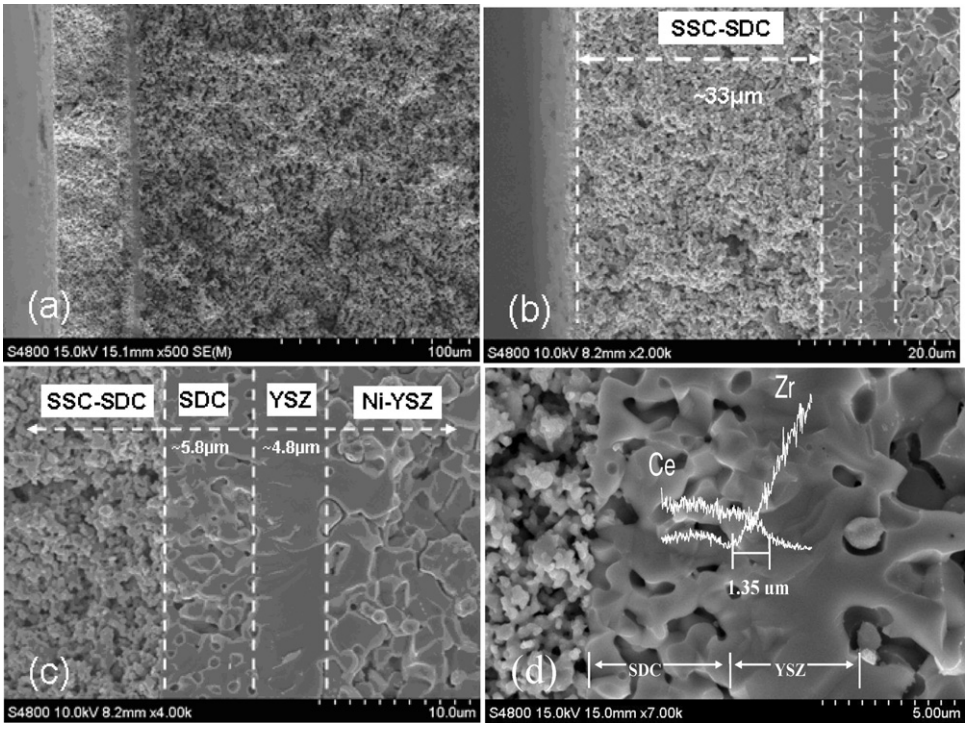

Fig. 3. SEM micrographs of the cross-sections of: (a) the whole cell; (b) SSC–SDC cathode; (c) SDC barrier and YSZ electrolyte; (d) the EDS analysis of the interface between YSZ and SDC.

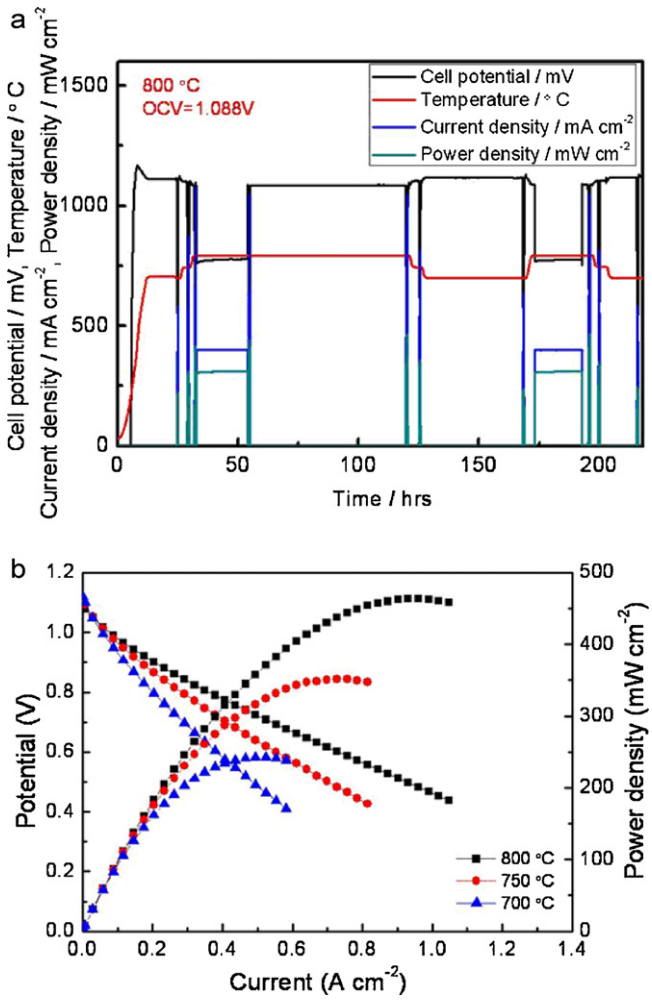

Fig. 4. (a) The whole process of the cell performance test and (b) I–*V* and *I*–*P* curves of the Ni–YSZ/YSZ/SDC/SSC–SDC single cell at different temperatures.

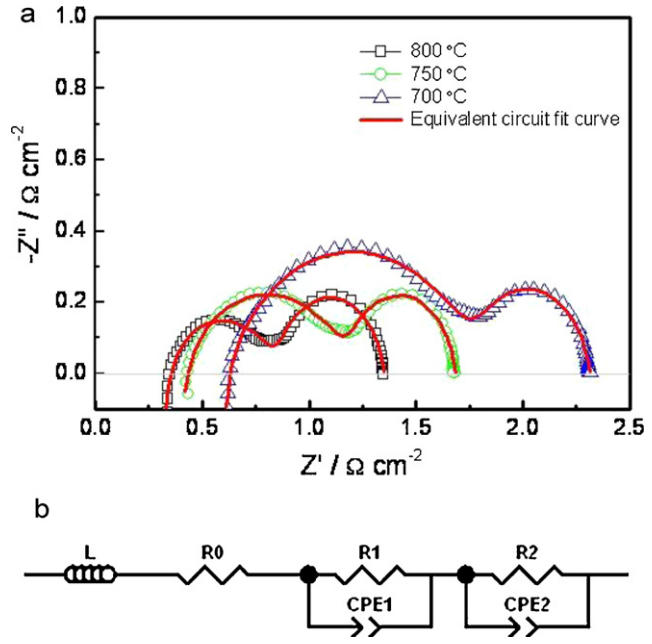

Fig. 5. (a) Impedance spectra measured at different temperatures and (b) equivalent circuit.

Table 1
The fitting results of the single cell operating at different temperatures.

Resistances ($\Omega\,cm^2$)	Temperature (°C)		
	700 °C	750 °C	800 °C
R_0	0.57	0.38	0.28
R_1	1.24	0.82	0.49
R_2	0.51	0.48	0.48

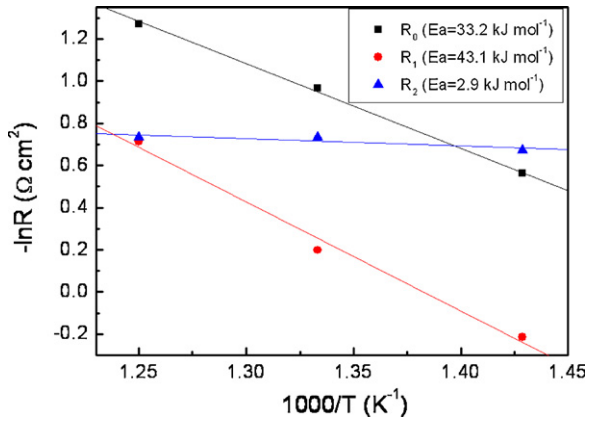

Fig. 6. Arrhenius plot of the polarization resistances measured at different temperatures.

ohmic resistance are increased with the decrease of the operating temperature. These results are in good agreement with those of the cell performance.

Fig. 6 shows the Arrhenius plots of polarization resistances for the cell. The activation energies of polarization resistances due to ohmic resistance of electrolyte, charge-transfer at the electrode/electrolyte interface (R1) and oxygen-reduction processes (R2) are estimated to be 33.2, 43.1, and 2.9 kJ mol^{-1}, respectively. This result shows that the activation energy of R1 is larger than other activation energies, which indicates that the interfacial resistance might be the most critical factor for the cell performance. The activation energy of R2 is very small, which shows that the SSC cathode possesses highly catalytic activity for oxygen-reduction reaction even at 700 °C. It is not necessary to increase the temperature to enhance the cathodic reaction of oxygen.

4. Conclusions

The single-phase SSC with perovskite structure can be obtained at a temperature above 1100 °C. The SEM shows that the dense YSZ electrolyte layer exhibits the good interfacial contact with both the Ni–YSZ and the SDC barrier. The porous SSC–SDC cathode shows an excellent adhesion with the SDC barrier. For the cell performance, the maximum power densities are 463.61, 351.28 and 242.96 mW cm^{-2} at 800, 750 and 700 °C, respectively. The impedances of the SSC–SDC cathode for the charge-transfer resistances (R_1) of the electrodes were 0.49, 0.82 and 1.24 $\Omega\,cm^2$, and the non charge-transfer resistances (R_2) were 0.48, 0.48 and 0.51 $\Omega\,cm^2$ at 800, 750 and 700 °C, respectively. The activation energies of R_1 and R_2 were estimated to be approximately 43.1 kJ $mole^{-1}$ and 2.9 kJ $mole^{-1}$, respectively. This result identifies that the SSC cathode material is compatible with the YSZ electrolyte via a delicate scheme to overcome the problems of the mechanical mismatch and material interactions within the MEA and obtain a noticeable performance of the SOFC.

References

[1] B.C.H. Steels, A. Heinzel, Nature 414 (2001) 345–352.
[2] E. Ivers-Tiffee, A. Weber, D. Herbstritt, J. Eur. Ceram. Soc. 21 (2001) 1805–1811.
[3] S.C. Singhal, Solid State Ionics 135 (2000) 305–313.
[4] Y.L. Yang, C.L. Chen, S.Y. Chen, C.W. Chu, A.J. Jacobson, J. Electrochem. Soc. 147 (2000) 4001–4007.
[5] Y. Liu, W. Rauch, S. Zha, M. Liu, Solid State Ionics 166 (2004) 261–268.
[6] E. Perry Murray, M.J. Sever, S.A. Barnett, Solid State Ionics 148 (2002) 27–34.
[7] Z. Shao, S.M. Haile, Nature 431 (2004) 170–173.
[8] Z. Shao, W. Yang, Y. Cong, H. Dong, J. Tong, G. Xiong, J. Membr. Sci. 172 (2000) 177–188.
[9] Q. Zhu, T. Jin, Y. Wang, Solid State Ionics 177 (2006) 1199–1204.
[10] S.B. Adler, Solid State Ionics 135 (2000) 603–612.
[11] A. Petric, P.H.F. Tietz, Solid State Ionics 135 (2000) 719–725.
[12] W. Zhu, Z. Lu, S. Li, B. Wei, J. Miao, X. Huang, K. Chen, N. Ai, W. Su, J. Alloy Compd. 465 (2008) 274–279.
[13] F.S. Baumann, J. Maier, J. Fleig, Solid State Ionics 179 (2008) 1198–1204.
[14] T. Ishihara, M. Honda, T. Shibayama, H. Minami, H. Nishiguchi, V. Takita, J. Electrochem. Soc. 450 (9) (1998) 3177–3183.
[15] H. Fukunaga, M. Koyama, N. Takahashi, C. Wen, K. Yamada, Solid State Ionics 132 (2000) 279–285.
[16] H.Y. Tu, Y. Takeda, N. Imanishi, O. Yamamoto, Solid State Ionics 100 (1997) 283–288.
[17] C. Xia, W. Rauch, F. Chen, M. Liu, Solid State Ionics 149 (2002) 11–19.
[18] W.X. Kao, M.C. Lee, T.N. Lin, C.H. Wang, Y.C. Chang, J. Power Sources 195 (2010) 2220–2223.
[19] W.X. Kao, M.C. Lee, Y.C. Chang, T.N. Lin, C.H. Wang, J.C. Chang, J. Power Sources 195 (2010) 6468–6472.
[20] Z. Tang, Y. Xie, H. Hawthorne, D. Ghosh, J. Power Sources 157 (2006) 385–388.
[21] N.P. Bansal, Z. Zhong, J. Power Sources 158 (2006) 148–153.
[22] A. Martinez-Amesti, A. Larrañaga, Lide.M. Rodriguez-Martinez, M.L. No, J.L. Pizarro, A. Laresgoiti, M.I. Arriortua, J. Power Sources 192 (2009) 151–157.
[23] Q.A. Huang, R. Hui, B. Wang, J. Zhang, Electrochim. Acta 52 (2007) 8144–8164.